Pattern formation in intracavity second-harmonic generation

C. Etrich, U. Peschel, and F. Lederer
Institut für Festkörpertheorie und Theoretische Optik, Friedrich-Schiller-Universität Jena, Max-Wien-Platz 1, 07743 Jena, Germany
(Received 2 April 1997)

We consider transverse effects in a planar resonator with a quadratically nonlinear medium where the incident field is at the fundamental frequency. The resonator is assumed to be resonant for both the fundamental and second harmonics. Different scenarios of destabilization of the plane-wave solutions are investigated in dependence on the driving field and the detunings from the resonances. Numerical simulations demonstrate the existence of dynamical and stationary patterns. [S1063-651X(97)11110-2]

PACS number(s): 42.65.Sf, 42.65.Ky, 42.65.Pc

I. INTRODUCTION

Planar resonators filled with nonlinear media are basic configurations in nonlinear optics. Due to their inherent feedback, they exhibit dynamical instabilities leading to fundamental spatiotemporal effects such as bistability, self-oscillations, or pattern formation [1–4]. Planar resonators provide a considerable field enhancement within the cavity that reduces the power requirements as far as the experimental verification of above-mentioned effects is concerned.

Various types of nonlinearities, which manifest themselves by the material placed in the cavity, were considered (see, e.g., [1–4] and references therein). Most extensively studied was the local and instantaneous cubic (Kerr) nonlinearity [1–3]. In the defocusing case optical plane-wave bistability can be observed [5]. In the focusing case the field tends to collapse in two-dimensional geometries. To obtain stationary patterns a saturation has to be included into the model [6].

In the case of a second-order nonlinearity phase and amplitude modulation are induced by the interaction of the fundamental and second-harmonic waves. In the limiting case of a weak second harmonic the problem can be reduced to the evolution of the fundamental with an effective cubic nonlinearity. Thus similar effects are expected to be found. But the second field introduces additional degrees of freedom and new effects evolve. For instance, the nonlocal interaction saturates for strong focusing due to the enhanced diffraction of the second harmonic and no collapse occurs even for free-space propagation [7]. Furthermore, the competition between the fundamental and second harmonics may give rise to additional dynamical instabilities (Hopf bifurcation) [8].

The aim of this work is to study the instabilities that occur in a planar resonator in the course of second-harmonic generation and their consequences. In contrast to the optical parametric oscillator (OPO) [4,9–11], we focus on incident fields at the fundamental frequency. Stable states are then characterized by mutually locked solutions at both frequencies (e.g., dichromatic patterns). For the fundamental the part of the total energy that is in the second harmonic plays the role of a nonlinear loss that corresponds to two-photon absorption in the case of a cubic nonlinearity with a complex-valued coefficient [12]. The optical response of the resonator is described by the well-established modal theory [13,14]. Compared with models based on forward- and backward-propagating fields, this simplifies the analysis considerably. It was shown that the modal theory decribes the response of an arbitrary planar resonator appropriately, provided the finesse is sufficiently high and thus the response is governed by a single resonance.

This paper is organized as follows. After the introduction of the basic equations in Sec. II we consider the stability of plane-wave solutions against spatially homogeneous and modulated pertubations in Sec. III. The formation of patterns is examined in Sec. IV. Finally, Sec. V concludes the paper.

II. BASIC EQUATIONS

We consider a Fabry-Pérot resonator with a quadratically nonlinear medium. Here the frequency of the incident fundamental field should be close to a resonance. Also, the generated second harmonic should interact with another resonance at approximately twice the fundamental frequency. Thus the system is resonant for both fields and a modal theory can be applied. In this way the field profile perpendicular to the resonator is assumed to be stationary and enters the evolution equations for the transmitted fields only via overlap integrals in the effective nonlinear coefficients. The absolute value of the overlap integrals depends critically on the phase mismatch between the fundamental and second harmonics and their mode profiles. The appropriately scaled evolution equations for the slowly varying envelopes A_1 and A_2 of the transmitted fields of the fundamental and second harmonics are derived analogously to the case of a cubic nonlinearity as [14]

$$i\frac{\partial A_1}{\partial T}+\frac{\partial^2 A_1}{\partial X^2}+\frac{\partial^2 A_1}{\partial Y^2}+(\Delta_1+i)A_1+A_1^* A_2=E, \quad (1a)$$

$$i\frac{\partial A_2}{\partial T}+\alpha\left(\frac{\partial^2 A_2}{\partial X^2}+\frac{\partial^2 A_2}{\partial Y^2}\right)+(\Delta_2+i\gamma)A_2+A_1^2=0, \quad (1b)$$

where Δ_1 and Δ_2 are the detunings of the two fields from the corresponding resonances. Though they have nothing to do with the common phase mismatch, they play a similar role in Eqs. (1). The time T is scaled in terms of the photon lifetime at the fundamental frequency and the spatial variables X and Y in terms of the square root of the product of the velocity of light, photon lifetime, and fundamental wavelength. Thus γ is the ratio of the photon lifetimes and α half the ratio

of the refractive indices corresponding to the fundamental and second harmonics. Throughout the analysis we assume $\alpha=1/2$, which is a very good approximation for realistic configurations. The input field of the fundamental is E, where an arbitrary phase can be transformed away.

The fields are scaled in terms of the effective nonlinear coefficients arising from the above-mentioned overlap integrals and the nonlinear material coefficients. For large absolute values of the detuning of the second harmonic different signs result in effective focusing ($\Delta_2<0$) or defocusing ($\Delta_2>0$) behavior. This is evident from neglecting the derivatives in Eq. (1b) for large Δ_2 and substituting for A_2 in Eq. (1a), leading to a cubic term there (see below).

III. HOMOGENEOUS STEADY-STATE SOLUTIONS AND THEIR STABILITY

As a prerequisite for the formation of patterns we consider the homogeneous steady-state or plane-wave solutions A_{n0}, $n=1,2$, of Eqs. (1) and their stability against spatially homogeneous and modulated perturbations. The plane-wave solutions are obtained by equating the derivatives in Eqs. (1) to zero [15]. This yields for the fields

$$\left(\Delta_1+i-\frac{1}{\Delta_2+i\gamma}|A_{10}|^2\right)A_{10}=E, \tag{2a}$$

$$(\Delta_2+i\gamma)A_{20}=-A_{10}^2. \tag{2b}$$

From this the equations for the moduli of the fields are

$$[|A_{10}|^4+2(\gamma-\Delta_1\Delta_2)|A_{10}|^2+(\Delta_1^2+1)(\Delta_2^2+\gamma^2)]|A_{10}|^2 =(\Delta_2^2+\gamma^2)E^2, \tag{3a}$$

$$|A_{20}|\sqrt{\Delta_2^2+\gamma^2}=|A_{10}|^2. \tag{3b}$$

For certain parameter ranges Eq. (3a) has three real solutions for $|A_{10}|^2$, which is a prerequisite for bistable behavior (see below). Equation (2a) is reminiscent of the case of a cubic nonlinearity with a complex-valued nonlinear coefficient, the imaginary part of which describes two-photon absorption [12]. Here it corresponds to a nonlinear loss of the fundamental due to the part of the total energy that is carried by the second harmonic and leaks out of the cavity because of radiation damping (proportional to γ).

A. Homogeneous stability

To determine the stability against spatially homogeneous perturbations, i.e., omitting the spatial derivatives in Eqs. (1), we substitute $A_n=A_{n0}+\delta A_n e^{\lambda T}$ into Eqs. (1) and linearize with respect to δA_{n0}. This leads to an eigenvalue problem for the propagation constant λ with the characteristic equations

$$\lambda^4+a_3\lambda^3+a_2\lambda^2+a_1\lambda+a_0=0, \tag{4}$$

where

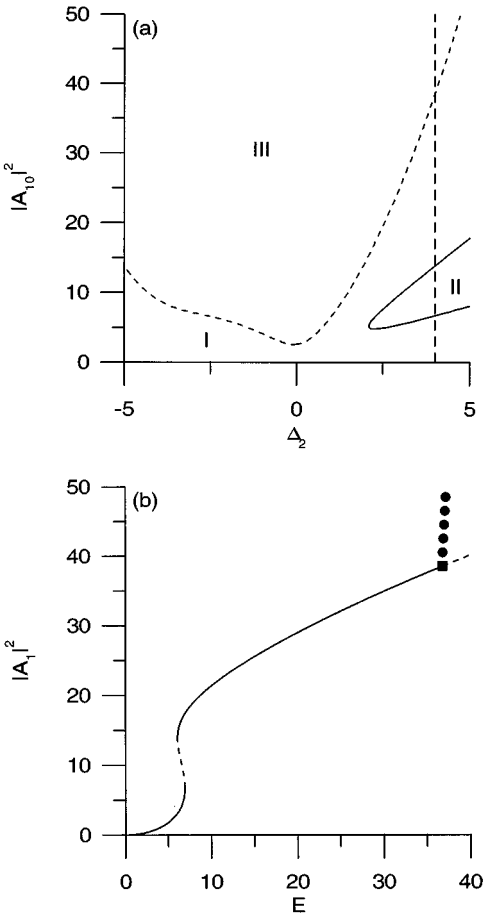

FIG. 1. (a) Loci of limit points (solid line) and Hopf bifurcations (dashed line) in the $(\Delta_2,|A_{10}|^2)$ plane for plane-wave solutions ($\Delta_1=4$ and $\gamma=0.6$) and (b) bifurcation diagram corresponding to the vertical dashed line in (a) ($\Delta_2=4$, solid lines correspond to homogeneously stable and dashed lines to homogeneously unstable plane-wave solutions; filled circles mark the maxima of stable periodic solutions and the square a Hopf bifurcation).

$$a_3=2(1+\gamma),$$

$$a_2=4(|A_{10}|^2+\gamma)-|A_{20}|^2+\Delta_1^2+1+\Delta_2^2+\gamma^2,$$

$$a_1=2[2(1+\gamma)|A_{10}|^2-\gamma|A_{20}|^2+\gamma(\Delta_1^2+1)+\Delta_2^2+\gamma^2],$$

$$a_0=4(|A_{10}|^2+\gamma-\Delta_1\Delta_2)|A_{10}|^2-(\Delta_2^2+\gamma^2)|A_{20}|^2 +(\Delta_1^2+1)(\Delta_2^2+\gamma^2).$$

Thus a plane-wave solution is unstable if Eq. (4) has a solution with $\mathrm{Re}\lambda>0$. A solution $\mathrm{Re}\lambda=0$, with either $\mathrm{Im}\,\lambda=0$ or $\mathrm{Im}\,\lambda\neq0$, marks a critical point in parameter space. Here there may be a transition from stable to unstable behavior. Equation (4) has a solution $\lambda=0$ if

$$|A_{10}|^2=\frac{2}{3}(\Delta_1\Delta_2-\gamma)\pm\frac{1}{3}\sqrt{(\Delta_1\Delta_2-\gamma)^2-3(\gamma\Delta_1+\Delta_2)^2}. \tag{5}$$

This corresponds to a pair of limit points, which mark the boundaries of a bistable domain, given that

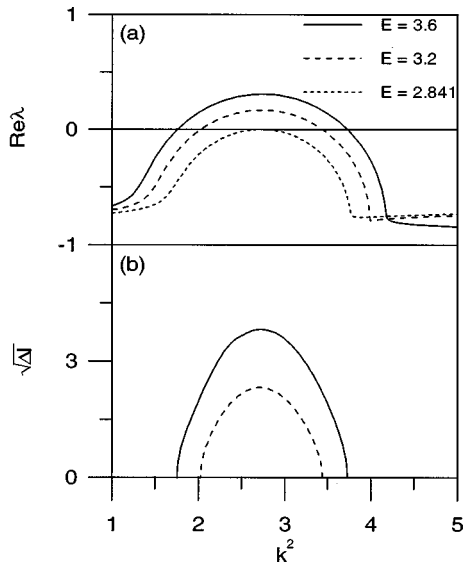

FIG. 2. (a) Reλ and (b) square root of the total relative intensity $[\Delta I=\int_0^P d\xi(|A_1-A_{10}|^2+|A_2-A_{20}|^2)$, P period] of traveling-wave solutions versus k^2 for various values of E [$\Delta_1=2$, $\Delta_2=2$, $\gamma=0.6$, and $k=2\pi/P$ in (a)].

$$\frac{|\Delta_2|(|\Delta_1|-\sqrt{3})}{\sqrt{3}|\Delta_1|+1}>\gamma, \quad \Delta_1\Delta_2>0. \tag{6}$$

From Eq. (6) an additional condition is obviously $|\Delta_1|>\sqrt{3}$. Furthermore, the plane-wave solutions destabilize via a Hopf bifurcation, which corresponds to a solution of the characteristic equation with $\mathrm{Re}\lambda=0$, $\mathrm{Im}\lambda\neq 0$. Thus substituting $\lambda=\pm i\omega_c$ into the characteristic equation and separating real and imaginary parts, the Hopf bifurcation is determined through

$$|A_{10}|^2=\frac{\gamma}{2(1+\gamma)^2}\left\{|A_{20}|^2-[(1+\gamma)^2+(\Delta_1+\Delta_2)^2]+4\Delta_2(\Delta_1+\Delta_2)+4\Delta_2^2\frac{(1+\gamma)^2+(\Delta_1+\Delta_2)^2}{|A_{20}|^2-[(1+\gamma)^2+(\Delta_1+\Delta_2)^2]}\right\}, \tag{7a}$$

$$\omega_c^2=a_1/a_3, \tag{7b}$$

where the square of the frequency ω_c with which the periodic solutions emanate from the Hopf bifurcation must be positive. Note that above condition is independent of whether the resonator is driven by the fundamental or second harmonic. Thus it holds also for the case of the OPO. In our case we have from Eq. (3b) $|A_{10}|^2=|A_{20}|\sqrt{\Delta_2^2+\gamma^2}$. Thus the Hopf bifurcation can be obtained as an intersection point of the two curves defined by Eqs. (3b) and (7a). From this we always found (numerically) two intersection points with one yielding a positive ω_c^2, thus leaving one Hopf bifurcation.

A typical example of the loci of critical points, i.e., limit points and Hopf bifurcations, in parameter space [in the $(\Delta_2,|A_{10}|^2)$ plane, which can be directly transformed to the (Δ_2,E) plane by means of Eq. (3a)] is displayed in Fig. 1 together with a bifurcation diagram in terms of the control parameter E. If Eqs. (3a) yield three real solutions for a certain range of E, the homogeneous steady-state solutions show bistable behavior, destabilizing at the first limit point and stabilizing at the second. They destabilize again at a Hopf bifurcation [cf. Fig. 1(b) and dashed line in Fig. 1(a)]. The plane-wave solutions are then stable in domain I of Fig. 1(a) and are unstable due to limit points in domain II and due to a Hopf bifurcation in domain III. The stability behavior of the periodic solutions bifurcating from the Hopf bifurcation is very complex and not considered here [8]. If Eqs. (3) yield only one real solution for all E, the homogeneous steady states destabilize via a Hopf bifurcation.

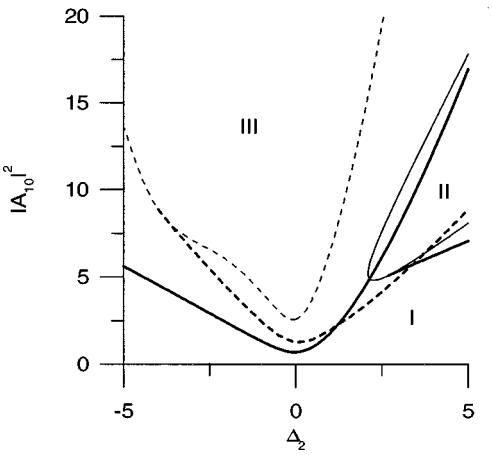

FIG. 3. Loci of critical points $[\mathrm{Re}\lambda(k^2)=0]$ in the $(\Delta_2,|A_{10}|^2)$ plane for plane-wave solutions ($\Delta_1=4$ and $\gamma=0.6$). Solid lines, $\mathrm{Im}\lambda(k^2)=0$; dashed lines, $\mathrm{Im}\lambda(k^2)\neq 0$; thin lines, $k=0$; bold lines, $k\neq 0$.

B. Modulational instabilities

Here we determine the stability of the homogeneous steady-state solutions against perturbations $A_n=A_{n0}+\delta A_n e^{\lambda T}e^{ik_X X+ik_Y Y}$, i.e., taking into account spatial modulations. We proceed in the same way as in Sec. III A, linearizing Eqs. (1) with respect to δA_{n0}. The corresponding characteristic equation can be obtained from Eqs. (4) by replacing Δ_1 and Δ_2 by Δ_1-k^2 and $\Delta_2-\alpha k^2$ with $k^2=k_X^2+k_Y^2$. Thus the coefficients become functions of k^2,

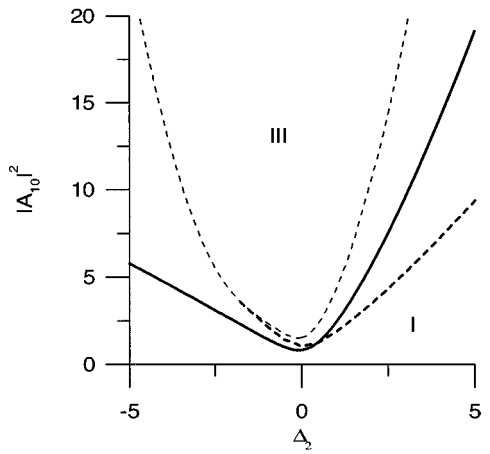

FIG. 4. Loci of critical points $[\mathrm{Re}\lambda(k^2)=0]$ in the $(\Delta_2,|A_{10}|^2)$ plane for plane-wave solutions ($\Delta_1=2$ and $\gamma=0.6$). Graphical conventions are as in Fig. 3.

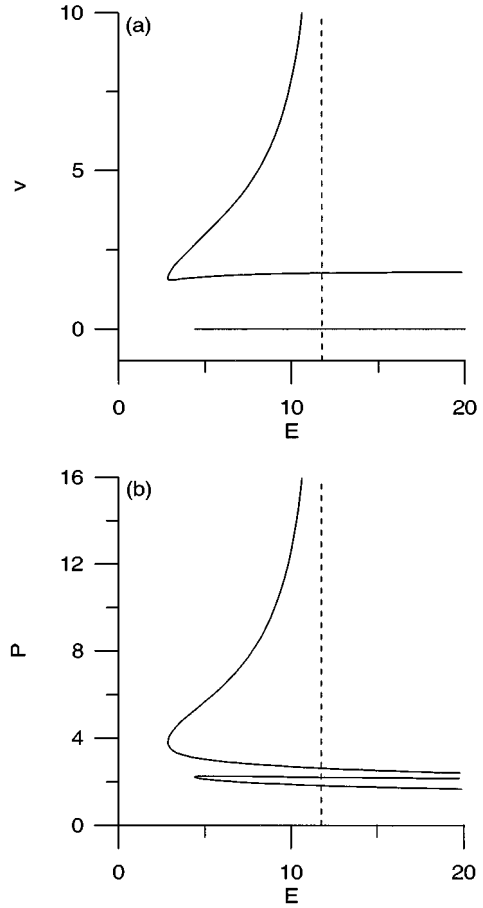

FIG. 5. Loci of Hopf bifurcations of Eqs. (10) (a) in the (E,v) plane and (b) in the (E,P) plane for $\Delta_1=2$, $\Delta_2=2$, and $\gamma=0.6$.

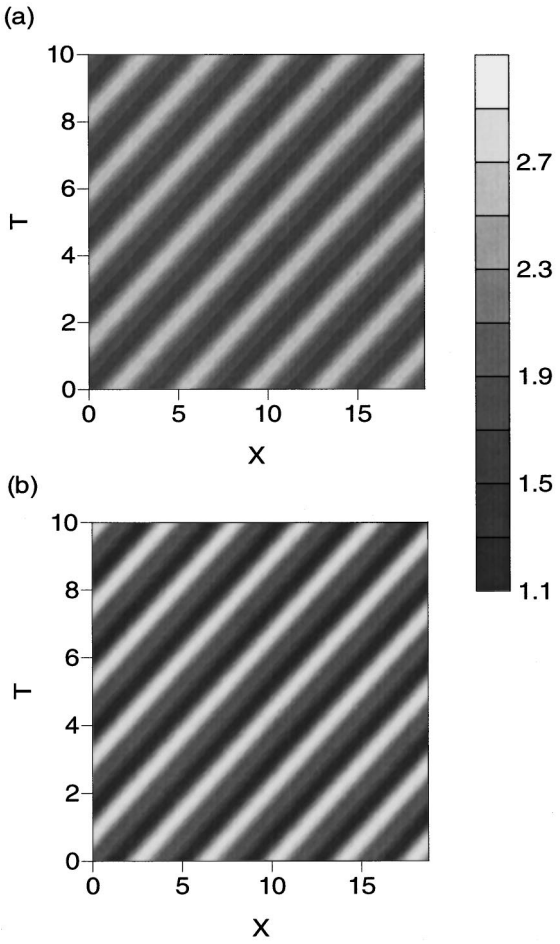

FIG. 6. Amplitude gray scale plots of the (a) fundamental and (b) second harmonics for $\Delta_1=2$, $\Delta_2=2$, $\gamma=0.6$, and $E=3.6$ displaying a traveling-wave solution.

i.e., $a_n=a_n(k^2)$. Correspondingly, the solutions of the characteristic equation are $\lambda=\lambda(k^2)$. We consider destabilization of the plane-wave solutions at finite k. As for $k=0$ there are two cases: $\mathrm{Re}\lambda(k^2)=0$ with either $\mathrm{Im}\lambda(k^2)\neq 0$ or $\mathrm{Im}\lambda(k^2)=0$.

Asymptotically, for $k^2\to\infty$, the solutions of the characteristic equation are

$$\lambda_{1,2}(k^2)=-1\pm i\left(k^2+\frac{\alpha(\alpha\Delta_1+\Delta_2)}{2-\alpha^2}\right)+O(1/k^2),$$
$$\lambda_{3,4}(k^2)=-\gamma\pm i\left(k^2\mp\frac{\alpha\Delta_1+\Delta_2}{1-2\alpha^2}\right)+O(1/k^2), \tag{8}$$

i.e., the plane-wave solutions are stable for sufficiently large k. Thus a plane-wave solution that is stable for $k=0$ [i.e., $\mathrm{Re}\lambda(0)<0$] destabilizes or becomes modulationally unstable where a local maximum of the corresponding $\mathrm{Re}\lambda(k^2)$ becomes positive [Fig. 2(a)]. Adding the loci in parameter space of these points to the example of Fig. 1(a) results in Fig. 3, leaving the plane-wave solutions stable in domain I. An example for a smaller value of Δ_1 is displayed in Fig. 4. Here the domain of bistability is at large Δ_2 and thus outside the figure. Figures 3 and 4 depict typical situations in parameter space. The critical points where the modulational instability sets in with $\mathrm{Im}\lambda(k^2)=0$ (bold solid lines) can easily be calculated from

$$a_0(k^2)=0,\quad \frac{da_0}{dk^2}=0, \tag{9}$$

solving for (real) $|A_{10}|^2$ and k^2 after substitution of Eq. (3b) and keeping the system parameters fixed. The first condition arises from $\lambda(k^2)=0$ [remember $\mathrm{Im}\lambda(k^2)=0$] and the second refers to the destabilization at the maximum mentioned above. Concerning Fig. 3, it should be noted that the plane-wave bistability is prevented due to a modulationally unstable upper branch.

IV. PATTERN FORMATION

Where the homogeneous steady states become modulationally unstable we expect patterns to develope: either traveling waves or roll patterns described by one vector (k_X,k_Y) or hexagons described by two linearly independent vectors (k_X,k_Y). Stable traveling waves may develop where the plane-wave solutions destabilize with $\mathrm{Im}\lambda(k^2)\neq 0$ (cf. bold dashed lines in Figs. 3 and 4) and stable stationary patterns where they destabilize with $\mathrm{Im}\lambda(k^2)=0$ (cf. bold solid lines in Figs. 3 and 4).

We first consider the case of traveling waves and roll patterns, assuming $k_X=k$ and $k_Y=0$. Traveling waves emanate from a critical point $\mathrm{Re}\lambda(k^2)=0$ with velocity

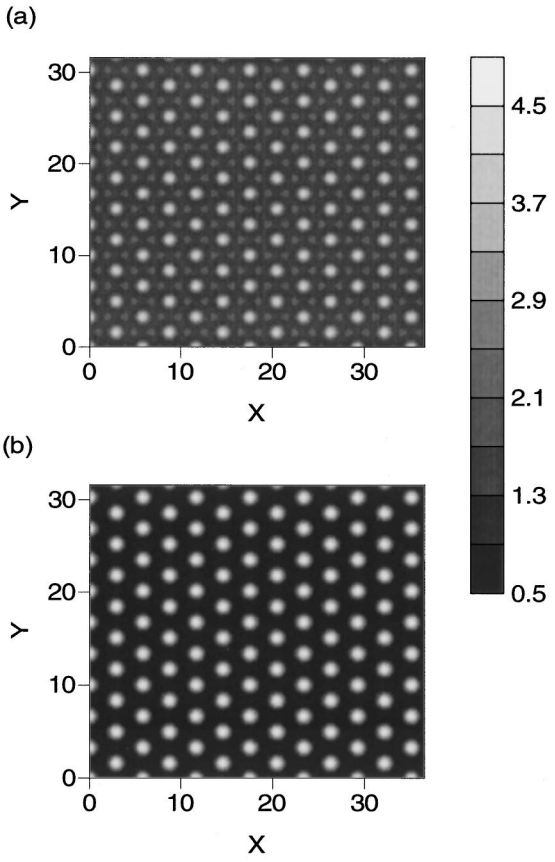

FIG. 7. Amplitude gray scale plots of the (a) fundamental and (b) second harmonics for $\Delta_1=2$, $\Delta_2=-1$, $\gamma=0.6$, and $E=6$ displaying a hexagon pattern.

$v=\mathrm{Im}\lambda(k^2)/k$ (remember $A_n=A_{n0}+\delta A_n e^{ik[X+\mathrm{Im}\lambda(k^2)/kT]}$). Roll patterns are included as a special case and correspond to $v=0$. Introducing the velocity v of traveling waves, they can be calculated as periodic solutions from

$$\frac{\partial^2 A_1}{\partial \xi^2}-iv\frac{\partial A_1}{\partial \xi}+(\Delta_1+i)A_1+A_1^* A_2=E,$$
$$\alpha\frac{\partial^2 A_2}{\partial \xi^2}-iv\frac{\partial A_2}{\partial \xi}+(\Delta_2+i\gamma)A_2+A_1^2=0, \tag{10}$$

which derives from Eqs. (1) assuming solutions with $\xi=X-vT$. With respect to Eqs. (10), the bifurcation behavior of traveling-wave solutions can be treated in terms of Hopf bifurcations in the usual way (as for $k=0$ in Sec. III, replacing the former time T by ξ). Such a Hopf bifurcation of Eqs. (10) corresponds to a critical point $\mathrm{Re}\lambda(k^2)=0$ of the original equations. Figure 5(a) displays the loci of Hopf bifurcations in the (E,v) plane. As pointed out above, at these points the velocity is $v=\mathrm{Im}\lambda(k^2)/k$ [in Fig. 5(a) only positive velocities are displayed]. The points where a local maximum of the corresponding $\mathrm{Re}\lambda(k^2)$ becomes positive are limit points in Fig. 5(a), i.e., if the control parameter E is increased beyond the limit point first encountered, the plane-wave solutions destabilize there. This happens with either $\mathrm{Im}\lambda(k^2)\neq 0$ $(v\neq 0)$ or $\mathrm{Im}\lambda(k^2)=0$ $(v=0)$. Note that in the case of roll patterns $(v=0)$ we have a limit point of two

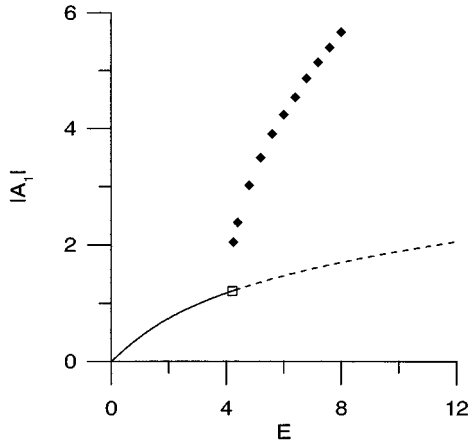

FIG. 8. Bifurcation diagram displaying the amplitude of the fundamental versus the control parameter E for $\Delta_1=2$, $\Delta_2=-1$, and $\gamma=0.6$. The rhombs represent the maximum available amplitude of hexagon patterns and the square marks the point where the modulational instability sets in.

degenerate branches. This becomes obvious if the period P of the periodic solutions of Eqs. (10) is used instead of v [Fig. 5(b)].

Fixing all parameters of Eqs. (1), for $v\neq 0$ the two Hopf bifurcations beyond the limit point are connected by a branch of traveling-wave solutions (the control parameter along the branch is v, each value of v corresponding to a certain period P of the traveling waves). They bifurcate from these points with period $P=2\pi/k$ [k from $\mathrm{Re}\lambda(k^2)=0$; cf. Fig. 5(b) with the velocity replaced by the period]. Examples of branches of traveling waves are shown in Fig. 2(b) for different values of E, together with $\mathrm{Re}\lambda(k^2)$ in Fig. 2(a). Here, for periodic solutions we defined $k=2\pi/P$. For roll patterns the situation is similar. For fixed E each of the degenerate

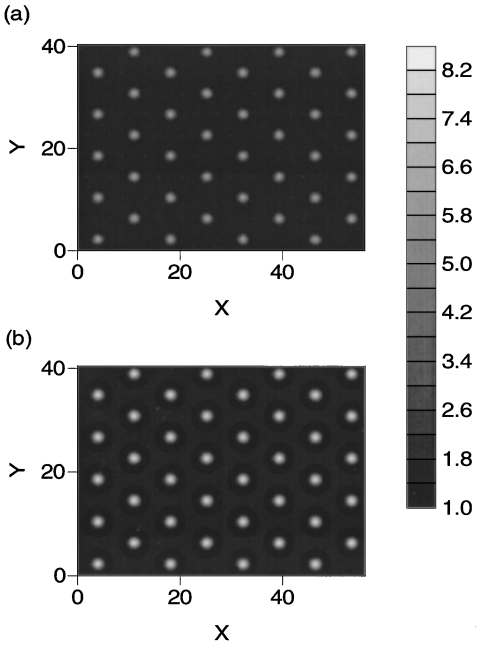

FIG. 9. Amplitude gray scale plots of the (a) fundamental and (b) second harmonics for $\Delta_1=-4$, $\Delta_2=-1.8$, $\gamma=0.6$, and $E=5.25$ displaying a hexagon pattern

branches corresponds to a bifurcation point with different period P [Fig. 5(b)]. The Hopf bifurcations described in Sec. III ($k=0$, homogeneous solutions) correspond to $v=\infty$, $P=\infty$ (cf. vertical dashed lines in Fig. 5).

Equations (10) do not yield the stability of the periodic solutions. This was tested by solving Eqs. (1) numerically. For the numerical simulations of pattern formation a split-step fast Fourier transform algorithm with periodic boundary conditions was used. Typical grid sizes were 128×128 points. In the example of Fig. 2(a) we found stable traveling-wave solutions around the maximum of $\mathrm{Re}\lambda(k^2)$ in k space. Increasing the control parameter E further, all traveling-wave solutions are unstable beyond a critical value of E. An example of a stable traveling-wave solution is displayed in Fig. 6. In the case of Fig. 3 there seem to be no stable traveling-wave solutions.

Concerning roll patterns, they seem to be unstable. Instead we found stable hexagonal patterns (for an example see Fig. 7) beyond the points where the plane-wave solutions destabilize with $\mathrm{Im}\lambda(k^2)=0$. Figure 8 displays an example of a branch of hexagonal patterns (plotted are the maximum amplitudes available). Here the hexagonal patterns seem to bifurcate with infinitesimal amplitude from the point where the plane-wave solutions become modulationally unstable. The intervals in k space where we find stable haxagonal patterns are shifted from the point where $\mathrm{Re}\lambda(k^2)$ $[\mathrm{Re}\lambda(k^2)>0]$ has its local maximum and are outside the interval with $\mathrm{Re}\lambda(k^2)>0$ close to the point where the modulational instability sets in. This seems to be similar to the findings for roll patterns in [11]. The situation is different for $\Delta_1<0$. For sufficiently negative Δ_2 (case of effective focusing) we find strongly localized hexagonal patterns that have finite amplitude just beyond the point where the plane-wave solutions become modulationally unstable (Fig. 9). The peak intensity of the second harmonic is considerably larger in this case.

V. CONCLUSION

We determined the stability behavior in parameter space of the homogeneous steady-state solutions. Neglecting spatial modulations, we found them always destabilizing via a Hopf bifurcation. Oscillating instabilities seem to play an essential role in resonators with a quadratically nonlinear medium. Taking into account spatial modulations, the Hopf bifurcations lead to traveling-wave solutions. Increasing the input power, they destabilize, resulting in more complicated motion. Roll patterns were always found to be unstable. Instead hexagons evolve. In the case of effective focusing they are extremely localized and have finite amplitude just beyond the point where the modulational instability sets in. The existence of the stable spatially modulated structures was demonstrated by means of two-dimensional numerical simulations. Modulational instabilities influence the plane-wave solutions considerably. There is no plane-wave bistability because we always found the upper branch of the bistable curve to be modulationally unstable. Thus switching from one homogeneous steady-state solution to another is not possible.

[1] N. B. Abraham and W. J. Firth, J. Opt. Soc. Am. B **7**, 951 (1990).
[2] L. A. Lugiato, Chaos Solitons Fractals **4**, 1251 (1994).
[3] L. A. Lugiato, Wang Kaige, and N. B. Abraham, Phys. Rev. A **49**, 2049 (1994).
[4] J. Opt. Soc. Am. B **10** (1993), special issue on optical parametric oscillation and amplification, edited by R. L. Byer and A. Piskarskas.
[5] W. J. Firth, I. Galbraith, and E. M. Wright, J. Opt. Soc. Am. B **2**, 1005 (1985).
[6] N. N. Rosanov and G. V. Khodova, J. Opt. Soc. Am. B **7**, 1057 (1990).
[7] W. E. Torruellas, Z. Wang, D. J. Hagan, E. W. Van Stryland, G. I. Stegeman, L. Torner, and C. R. Menyuk, Phys. Rev. Lett. **74**, 5036 (1995).
[8] Paul Mandel, N. P. Pettiaux, Wang Kaige, P. Galatola, and L. A. Lugiato, Phys. Rev. A **43**, 424 (1991).
[9] G.-L. Oppo, M. Brambilla, D. Camesasca, A. Gatti, and L. A. Lugiato, J. Mod. Opt. **41**, 1151 (1994).
[10] G.-L. Oppo, M. Brambilla, and L. A. Lugiato, Phys. Rev. A **49**, 2028 (1994).
[11] G. J. de Valcárcel, K. Staliunas, E. Roldán, and V. J. Sánchez-Morcillo, Phys. Rev. A **54**, 1609 (1996).
[12] G. I. Stegeman, D. J. Hagan, and L. Torner, Opt. Quantum Electron. **28**, 1691 (1996).
[13] R. Ulrich, J. Opt. Soc. Am. **60**, 1337 (1970).
[14] T. Peschel and F. Lederer, Phys. Rev. B **46**, 7632 (1992).
[15] R. Reinisch, E. Popov, and M. Nevière, Opt. Lett. **20**, 854 (1995).